Superconducting microbolometers for time-resolved terahertz spectroscopy

Daniel F. Santavicca, Anthony J. Annunziata, Matthew O. Reese, Luigi Frunzio, Daniel E. Prober*
Dept. of Applied Physics, Yale University, 15 Prospect St., New Haven, CT 06511

ABSTRACT

We report the characterization of superconducting niobium microbolometers designed for time-resolved terahertz spectroscopy on nanosecond to millisecond timescales. Coupling of the incident signal is achieved via a planar antenna mounted on a hyperhemispherical silicon lens. We have integrated these detectors into a custom Fourier-transform spectrometer. The spectrometer optics are frequency independent over the spectral range 0.1-3 terahertz and thus the system bandwidth is set by the detector antenna. We have fabricated devices with two different antenna geometries, the double-dipole and the log spiral, and have characterized the spectral response of each. This detector will enable a variety of novel spectroscopy applications.

Keywords: far-infrared, terahertz, bolometers, superconducting devices, time-resolved spectroscopy

1. INTRODUCTION

The superconducting microbolometer has been developed extensively over the past decade as a heterodyne mixer for submillimeter wavelength astronomy.[1] These detectors are designed to have high sensitivity and a large intermediate frequency bandwidth, typically several GHz. We have adapted this technology to develop direct detectors for applications in laboratory-based terahertz (THz) spectroscopy. These applications can make use of the high sensitivity and fast response time of the superconducting microbolometer, but they typically require greater power handling. The goal of this work is to develop a detector capable of performing sensitive time-resolved measurements on nanosecond to millisecond timescales. These timescales are too long for techniques utilizing a free space optical delay line but too short for a standard commercial bolometer.

Earlier work characterized the infrared response of large area niobium films.[2,3] By utilizing antenna-coupling to a small area Nb bolometer, we can minimize the active device volume and improve the sensitivity. Additionally, a planar antenna couples to a single electromagnetic mode, collecting much less background power than a large area, multi-mode detector. The development of an antenna-coupled niobium microbridge suspended over a vacuum gap has also been reported.[4,5] That device is designed for terahertz imaging applications. It demonstrated similar sensitivity but orders of magnitude slower response than the device we present. The inductance of the relatively long microbridge limits efficient coupling to below ≈ 1 THz. An antenna-coupled niobium bolometer for the spectral range 0.3-3 THz has recently been developed by Insight Product Co.[6] The specifications quote a similar response time and sensitivity to our device. We report here more detailed performance data, including the dependence of the responsivity on bath temperature and input power, as well as the frequency dependence of the output noise and the spectral response of the antenna.[7,8,9] These characterizations are intended to serve as a guide for future spectroscopy applications.

Together with the Fourier-transform spectrometer we describe, this detector can be used to study a variety of dynamic systems. One possibility is the study of time-dependent conductivity in semiconductor nanoparticles following a sub-ps optical excitation pulse. This type of measurement has already been performed on ps timescales using an optical delay line,[10,11] and our detector would enable the extension of these measurements to longer timescales. Other potential applications include studies of phonon relaxation[12] and the dynamics of highly excited molecules.[13] To perform such time-resolved measurements, the THz transmission through the sample or emission from the sample can be monitored in real time on an averaging oscilloscope following an initiating event such as an optical excitation pulse. This can be used to measure the frequency-averaged THz response without the use of an interferometer. Alternatively, an interferometer can be used to measure the time-dependent response at each point in the interferogram. This will give the time dependence of each spectral component within the measurement bandwidth.

*daniel.prober@yale.edu; phone 203-432-4280; fax 203-432-4283; yale.edu/proberlab

2. DEVICE OPERATION

The device consists of a niobium (Nb) microbridge spanning two much larger non-superconducting contacts, which are a bilayer of 12 nm of Nb and 200 nm of aluminum (Al). The contacts form an antenna for coupling the incident THz signal to the microbridge, as well as electrical leads for dc biasing and ac readout. The leads consist of a quarter-wave THz choke structure to minimize loss of the incident signal. The Nb-Al bilayer has a sheet resistance of less than 0.1 Ω/square. Typical microbridge dimensions are 2 μm wide, 5 μm long, and 12 nm thick. The bridge is designed to have a resistance of approximately 100 Ω to be well-matched to the antenna. Devices are fabricated on double-side polished, 200 μm thick, high-resistivity (>20 kΩcm) silicon substrates for quasi-optical coupling.[8] Optical micrographs of devices with two different antenna geometries are presented in Figure 1.

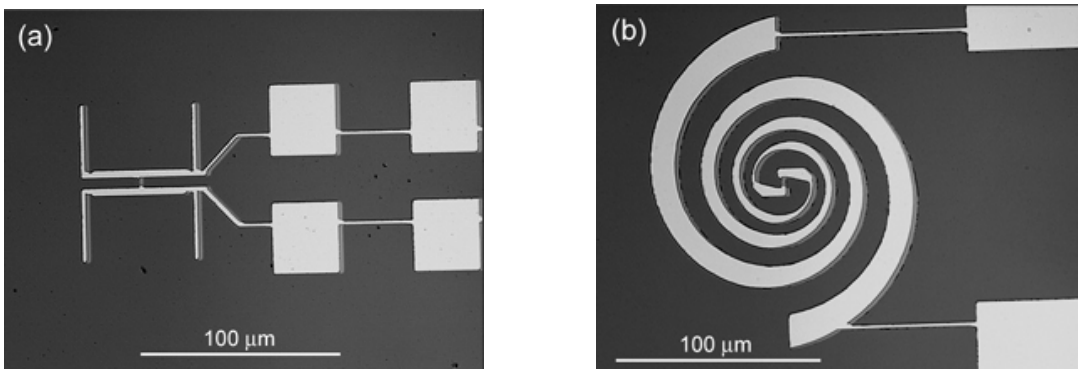

Fig. 1. Optical micrographs of devices with two antenna geometries: (a) 79 μm double-dipole, (b) log spiral. The niobium microbridge is in the center of each antenna, and the lead structure with quarter-wave choke is visible to the right.

The device is a sensitive bolometric detector when biased on its superconducting transition. Devices are cooled below the superconducting transition temperature of the microbridge and biased on the normal branch of the I-V curve with a 20 Ω dc load line. A typical resistance versus temperature curve and I-V curves are presented in Figure 2.

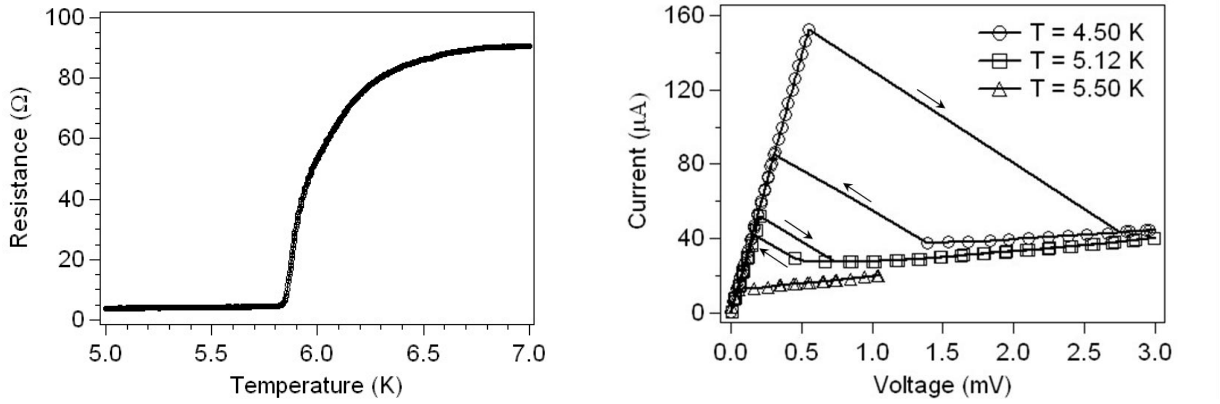

Fig. 2. Resistance versus temperature measured with I_{dc} = 1 μA (left), and current versus voltage measured at three different bath temperatures with a 20 Ω dc load line (right). Arrows indicate the direction of sweep for hysteretic curves.

Previous work on Nb mixers found that the response time is set by electron-phonon coupling in the Nb film for bridge lengths greater than approximately 1 μm.[14] For thin Nb at ~4 K, the electron-phonon time is proportional to T^{-2}, where T is the temperature of the electron system.[15] For a superconducting bolometer, the operating temperature is always approximately equal to the superconducting critical temperature T_c, and thus the thermal response time of the detector will be proportional to T_c^{-2}.

In a simple lumped-element model of bolometer performance, the responsivity S, in units of V/W, is given by $S = I_{dc}(dR/dT)/G$, where G is the thermal conductance between the electron system in the microbridge and the bridge/substrate phonons.[16] G was measured using Johnson noise thermometry to be 2.1 x 10^{-7} W/K at T = 6 K.[7] For I_{dc} = 20 μA and dR/dT = 100 Ω/K, we expect S ~ 10^4 V/W. In this model, the saturation power $P_{sat} = G\Delta T_c$, where ΔT_c is the width of the superconducting transition. For ΔT_c = 0.5 K, P_{sat} ~100 nW. As G is proportional to the bridge volume, P_{sat} should scale linearly with the volume.

Device sensitivity is typically specified as a noise equivalent power (NEP), which is the signal that can be resolved with a signal-to-noise ratio of one with a 1 Hz output bandwidth, in units of W/(Hz)$^{1/2}$. Noise sources include photon shot noise, thermal fluctuation noise, Johnson noise, and amplifier noise. These noise sources are assumed to be uncorrelated and hence the noise amplitudes add in quadrature. The NEP due to Johnson noise is $NEP_J = \sqrt{k_B T R}/S$, where R is the device resistance. For T = 6 K, R = 50 Ω, and S = 4 x 10^4 V/W, we get NEP_J = 1.6 x 10^{-15} W/(Hz)$^{1/2}$. An amplifier with a noise temperature T_N will contribute noise equivalent to a Johnson noise source at a physical temperature T_N. Presently available broadband rf amplifiers have noise temperatures of ~100 K at room temperature and ~10 K at cryogenic temperatures. The NEP due to photon shot noise from a blackbody background at temperature T in the Rayleigh-Jeans limit is $NEP_{photon} = \eta k_B T\sqrt{2B}$, where η is the optical coupling efficiency and B is the input bandwidth.[16] For η = 0.2, B = 1 THz, and T = 300 K, we get NEP_{photon} = 1.2 x 10^{-15} W/(Hz)$^{1/2}$. The thermal fluctuation noise is given by $NEP_{th} = \sqrt{4k_B T^2 G}$.[16] For T = 6 K, we get NEP_{th} = 2.0 x 10^{-14} W/(Hz)$^{1/2}$. Thus, given a sufficiently low noise amplifier, the thermal fluctuation noise should determine the device sensitivity.

Important figures of merit for any bolometer are speed, sensitivity, and saturation power. For our device, these have competing dependencies on the microbridge volume and critical temperature, both of which are a function of the microbridge geometry. These dependencies are summarized in Table 1. The optimum tradeoff between these competing parameters will depend on the requirements of a particular application.

Table 1. Dependence of sensitivity, saturation power, and time constant on bridge volume and critical temperature for a phonon-cooled Nb bolometer.

$NEP_{th} \propto volume^{1/2}, T_c^{5/2}$
saturation power ∝ volume
time constant ∝ T_c^{-2}

3. MICROWAVE CHARACTERIZATION

Microwave frequency performance was characterized with the device mounted in a vacuum can in a pumped ^{4}He cryostat. Negligible infrared radiation reached the device. The time constant was measured via a mixing measurement at a bath temperature of 4.2 K. The sum of two high frequency signals (f_1 = 1.4 GHz and f_2 = 1.5-2.4 GHz) was coupled to the device with a directional coupler, and the device response at the difference frequency ($f_2 - f_1$) was amplified by a broadband cryogenic amplifier (0.1-8 GHz) and measured on a spectrum analyzer. The mixer conversion efficiency as a function of the difference frequency is seen in Figure 3. The data are fit to a Lorentzian roll-off to get a -3 dB frequency f_{-3dB} = 240 MHz, which corresponds to a time constant $\tau = 1/(2\pi f_{-3dB})$ = 0.7 ns. This is consistent with previous measurements of the electron-phonon time in thin Nb films.[14,15]

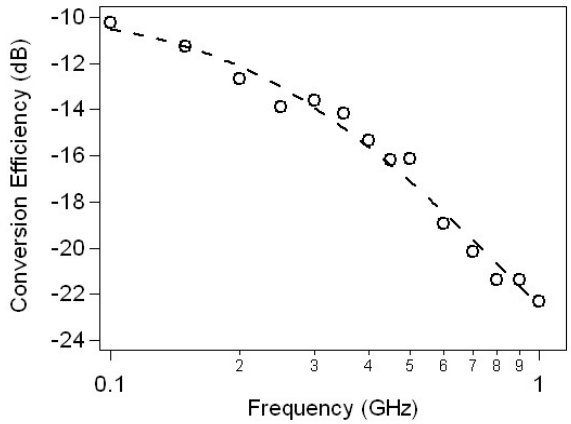

Fig. 3. Conversion efficiency versus difference frequency (circles) fit to a Lorentzian (dashed line) to determine the time constant $\tau = 0.7$ ns.

The responsivity at the optimum bias point as a function of signal power was measured by coupling to the device the sum of two ≈ 1 GHz signals separated by 80 MHz and measuring the device response at the difference frequency. The data for several different bath temperatures are presented in Figure 4. The largest responsivity is obtained for bath temperatures $\approx 0.9T_c$. At lower bath temperatures, the responsivity decreases but P_{sat} increases, where we define P_{sat} as the power at which the responsivity decreases by a factor of 2. The data approximately follow the empirical relation

$$S(P) = \frac{S(0)}{1 + (P / P_{sat})^{\alpha}} \tag{1}$$

where $\alpha = 1.5$ at T = 5.2 K and $\alpha = 2$ at T = 4.2 K and 3.2 K. The small-signal responsivity and saturation power obtained from fitting the data for each bath temperature to Equation 1 are summarized in Table 2.

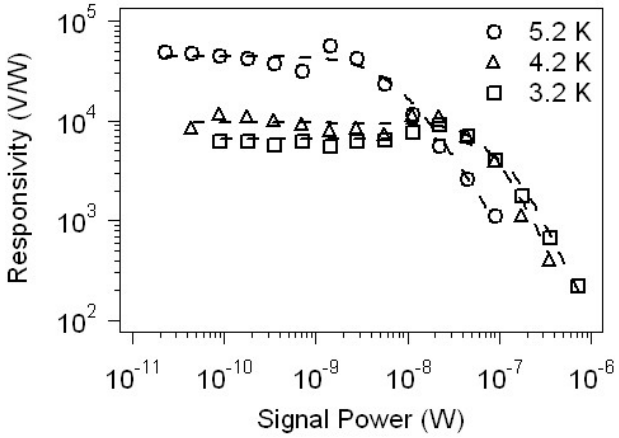

Fig. 4. Responsivity at the optimum bias point as a function of signal power at different bath temperatures. Dashed lines are a fit to Equation 1.

Table 2. Small signal responsivity and saturation power at different bath temperatures.

Bath temperature (K)	Small-signal Responsivity (V/W)	Saturation power (nW)
5.2	4.4×10^4	7
4.2	1.0×10^4	79
3.2	0.7×10^4	126

The output noise was measured as a function of frequency at a bath temperature of 5.2 K. At audio frequencies, we used a low-noise preamp with an input transformer. At microwave frequencies, we used a cryogenic 50 Ω amplifier. In each case, the amplifier noise temperature was calibrated *in-situ* using the Johnson noise of the device above T_c. At the optimum bias point, the measured device noise was flat from approximately 100 Hz to 100 MHz, corresponding to an NEP of 2.0 x 10^{-14} W/(Hz)$^{1/2}$. In this output bandwidth, the device operates near the limit of thermal fluctuation noise. Below 100 Hz, there is a 1/f-like rise. We note that the relatively low 1/f noise is favorable, as it permits measurements with a mechanical chopper to be performed with similar sensitivity to higher frequency measurements. Above 100 MHz, the noise rolls off with a frequency dependence that is similar to the device response, as expected.[7,13]

4. SPECTROMETER DESIGN

The device substrate is aligned and attached to the back of a 6 mm diameter hyperhemispherical silicon lens,[17] where the device is at the silicon-air interface. The device is electrically connected to the sample holder with wirebonds, and the sample holder is mounted in an optical-access ^{4}He cryostat. The cryostat window is a 90 μm thick Mylar sheet. A cooled Zitex G110 membrane, which absorbs strongly above 4 THz, serves as an infrared filter on the heat shield window.[18]

The spectrometer uses a silicon carbide globar as a hot blackbody source.[19] At a current of 5 A, the globar temperature is approximately 1000 K. The source is modulated by a room temperature chopping wheel, the surface of which has been coated with carbon-loaded epoxy. For a single-mode detector, the power from a blackbody at temperature T into a matched load is given by the 1D Planck spectrum

$$P = \frac{hf}{e^{hf/k_B T} - 1} \tag{2}$$

where f is the photon frequency. The power modulation between 300 K and 1000 K in the frequency range 0.5 – 1.5 THz is δP = 9.7 nW. At frequencies of order a terahertz and temperatures of order room temperature and higher, the source is in the Rayleigh-Jeans limit, in which Equation 2 simplifies to $P = k_B TB$, where B is the frequency bandwidth.

The size of the globar is defined by a 6 mm iris, and the signal is collimated with a 63.5 mm diameter 90^0 off-axis parabolic mirror.[20] The collimated signal is sent to a beamsplitter consisting of a 6 mm thick, 100 mm diameter high-resistivity silicon wafer.[21] The use of a thick beamsplitter allows for broadband, high-efficiency interferometry provided that the desired frequency resolution Δf is larger than approximately twice the etalon spacing.[22] For 6 mm thick Si (ε = 11.9), the etalon spacing is 7 GHz. A plot of the calculated power transmission versus frequency for normal incidence for the Si beamsplitter is presented in Figure 5, along with a plot of the calculated power transmission for 50 μm thick mylar (ε = 3.1) for comparison. These calculations neglect loss in the beamsplitter.

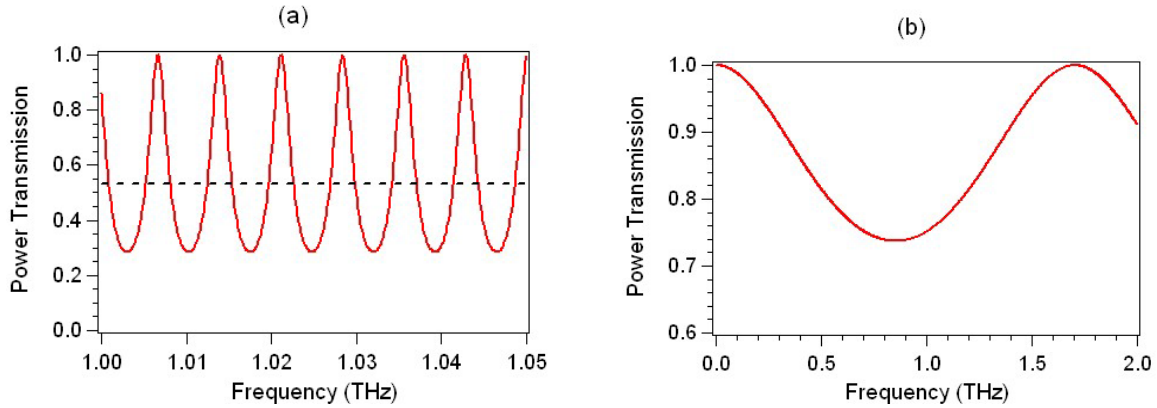

Fig. 5. (a) Calculated power transmission versus frequency for 6 mm Si beamsplitter showing etalon peaks (solid curve) and the average power transmission (dashed curve). (b) Caculated power transmission for a 50 μm mylar beamsplitter. Note the difference in scale on the frequency axis.

A fixed mirror and a moveable mirror define each arm of the interferometer. The moveable mirror is mounted on a linear translation stage driven by an Ealing EncoderDriver linear actuator with a range of motion of 10 mm, a resolution of 0.02 μm, and a repeatability of 0.1 μm. This range corresponds to a frequency resolution of 15 GHz, which should effectively average out the etalons from the beamsplitter. The combined signal from the two arms is focused onto the detector inside the cryostat with a second off-axis parabolic mirror. A mechanical chopper with a maximum chopping frequency of 400 Hz is positioned in front of the cryostat window. The entire system sits inside a nitrogen drybox to minimize absorption by water vapor. Maintaining a positive pressure of dry nitrogen gas overnight yields a relative humidity of approximately 2-4%. A schematic of the spectrometer is presented in Figure 6.

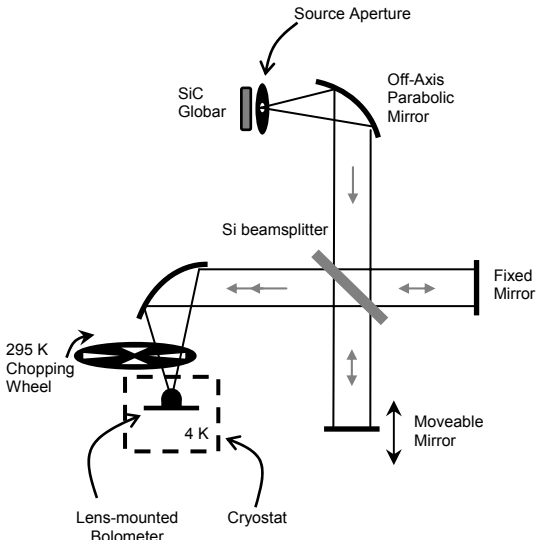

Fig. 6. Schematic of the Fourier-transform spectrometer.

The device signal at the chopping frequency is amplified by a low-noise voltage preamp. A 1:60 transformer steps up the device impedance to achieve optimum noise performance. A large inductor is used on the biasing line to minimize noise from the biasing electronics. The output of the preamp is coupled to a lock-in amplifier, which detects at the chopping frequency.

5. TERAHERTZ CHARACTERIZATION

The spectrometer was used to measure the spectral response of the two antennas pictured in Figure 1. The double-dipole antenna is designed so the two half-wave dipole elements radiate in-phase in the direction perpendicular to the substrate and out-of-phase in the direction parallel to the substrate.[23] A dipole in a dielectric half space radiates power preferentially into the high dielectric material in proportion to the square root of the dielectric constant, so our antenna should couple with approximately 80% efficiency from the lens side of the device.[24] The log spiral antenna is defined in polar coordinates by the equation $\rho(\phi) = ke^{a(\phi+\phi_0)}$. In our design, a = 0.15, each arm is defined by a shift $\varphi_0 = \pi/2$, and the shift between arms is π. The lower frequency limit of the log spiral bandwidth corresponds approximately to the total arm length, and the upper frequency limit is set by the finite size of the load.[25]

The device response as a function of mirror displacement was measured with a step size of 10 μm, corresponding to a maximum frequency of 7.5 THz. The time per step was 0.8 s and the lock-in time constant was 0.3 s. Typical scans for both antennas at 2-4% relative humidity are presented in Figure 7. The data presented are single scans, and the average (off-peak) device response has been subtracted from the data. The response is highly reproducible from scan to scan. The scan length of 6 mm corresponds to a frequency resolution of 25 GHz, and it takes approximately 8 minutes to acquire the data. The slight asymmetry in the interferograms is likely the result of imperfect alignment of the spectrometer.

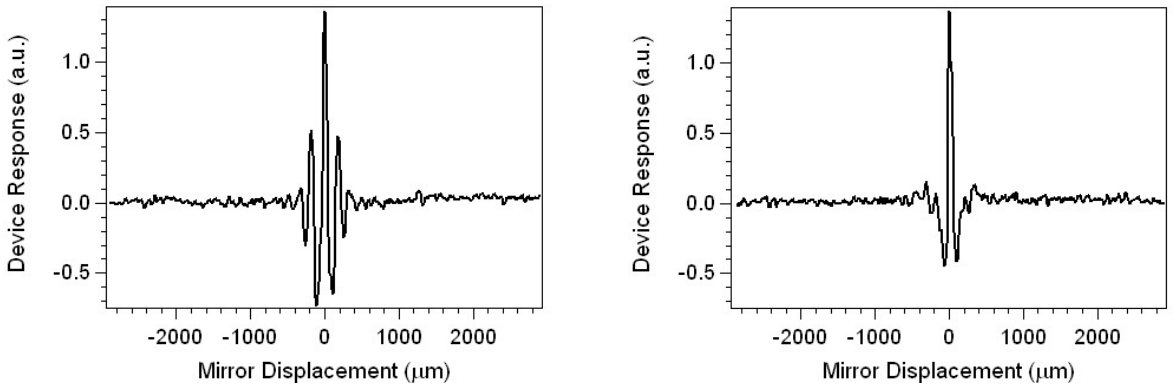

Fig. 7. Typical interferograms for 79 μm double-dipole antenna (left) and log spiral antenna (right).

The measured interferogram is Fourier transformed to get the spectral response. Normalized spectra from the two devices are presented in Figure 8. The irregular structure in each spectrum is highly reproducible and thus does not appear to be dominated by noise. The 0.8 THz response peak of the double-dipole response is approximately equal to the half-wave resonance of a 79 μm dipole in an effective dielectric that is equal to the mean of the dielectric constants of Si and air. The log spiral response has unanticipated attenuation at frequencies above 1 THz. The cause of this is unknown, although it may be due to a distortion of the antenna geometry that results from the fabrication process.[8,26] This issue, as well as other antenna geometries, will be investigated in future work.

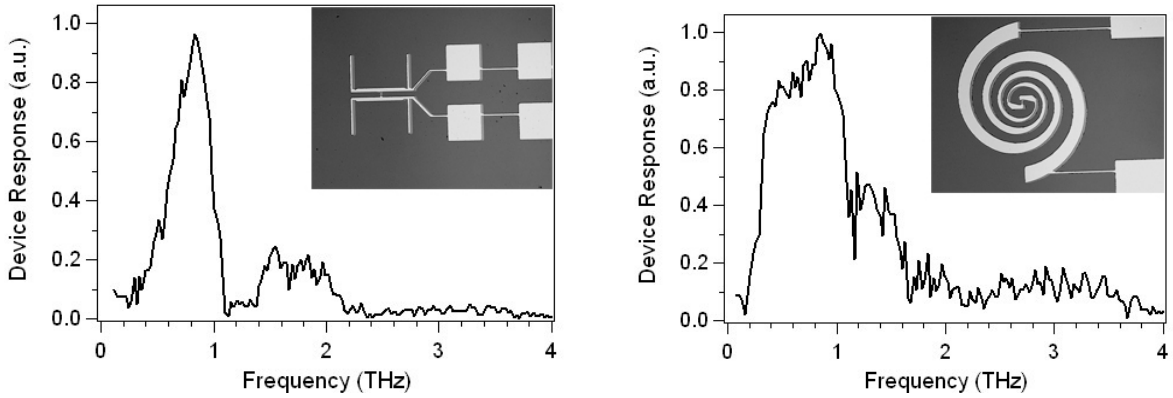

Fig. 8. Normalized spectra for device with 79 μm double-dipole antenna (left) and log spiral antenna (right) with optical device micrograph insets.

6. CONCLUSION

We have demonstrated a superconducting microbolometer with a sub-nanosecond response time and a sensitivity approaching the limit of thermal fluctuation noise. This detector was integrated into a custom Fourier-transform spectrometer, which was used to measure the bandwidths of two antenna geometries. This system can be used to perform time-resolved measurements of dynamic systems on nanosecond to millisecond timescales, enabling a variety of novel spectroscopy applications.

ACKNOWLEDGEMENTS

We thank J. Bae, J. Chudow, H. Drew, R. Grober, P. Pütz, B. Reulet, C. Schmuttenmaer, A. Skalare, A. True, and A. Young for assistance and helpful discussions. This work was supported by NSF-CHE-0616875, NSF-DMR-0407082, and Yale University. L.F. acknowledges partial support from the CNR-Istituto di Cibernetica, Pozzuoli, Italy.

REFERENCES

[1] J. Zmuidzinas and P. L. Richards, "Superconducting detectors and mixers for millimeter and submillimeter astrophysics," *Proc. IEEE* **92**, 1597-1616 (2004).

[2] E. M. Gershenzon, M. E. Gershenzon, G. N. Gol'tsman, A. D. Semyonov and A. V. Sergeev, "Heating of electrons in superconductor in the resistive state due to electromagnetic radiation," *Solid State Comm.* **50(3)**, 207-212 (1984).

[3] E. M. Gershenzon, G. N. Gol'tsman, B. S. Karasik, G. Ya. Lugova, N. A. Serebryakova and E. V. Chinkova, "IR radiation detectors based on electronic heating of films made from conventional superconductors in the resistive state," *Sverkhprovodimost'* (KIAE) **5**, 1129-1140 [*Supercond.* **5**, 1126-1137] (1992).

[4] A. Luukanen and J. P. Pekola, "A superconducting antenna-coupled hot-spot microbolometer," *Appl. Phys. Lett.* **82**, 3970-3972 (2003).

[5] A. Luukanen, E. N. Grossman, A. J. Miller, P. Helisto, J. S. Penttila, H. Sipola and H. Seppa, "An ultra-low noise superconducting antenna-coupled microbolometer with a room temperature read-out," *IEEE Microwave and Wireless Comp. Lett.* **16**, 464-466 (2006).

[6] Insight Product Co. (Newton, MA), http://www.insight-product.com

[7] D. F. Santavicca, M. O. Reese, A. B. True, C. A. Schmuttenmaer and D. E. Prober, "Antenna-coupled niobium bolometers for terahertz spectroscopy," *IEEE Trans. Appl. Supercond.* **17(2)**, 412-415 (2007).

[8] D. F. Santavicca, A. J. Annunziata, M. O. Reese, L. Frunzio and D. E. Prober, "A far-infrared Fourier-transform spectrometer with an antenna-coupled niobium bolometer," *Supercond. Sci. Technol.* **20**, to appear (2007).

[9] M. O. Reese, D. F. Santavicca, D. E. Prober, A. B. True and C. A. Schmuttenmaer, "Niobium direct detectors for fast and sensitive terahertz spectroscopy," *Rev. Sci. Instrum.* to appear (2007).

[10] J. B. Baxter and C. A. Schmuttenmaer, "Conductivity of ZnO nanowires, nanoparticles, and thin films using time-resolved terahertz spectroscopy," *J. Phys. Chem.* **110**, 25229-25239 (2006).

[11] D. G. Cooke, A. N. MacDonald, A. Hryciw, J. Wang, Q. Li, A. Meldrum and F. A. Hegmann, "Transient terahertz conductivity in photoexcited silicon nanocrystal films," *Phys.Rev. B* **73**, 19331 (2006).

[12] G. Haran, W.-D. Sun, K. Wynne and R. M. Hochstrasser, "Femtosecond far-infrared pump-probe spectroscopy: a new tool for studying low-frequency vibrational dynamics in molecular condensed phases," *Chem. Phys. Lett.* **274**, 365-371 (1997).

[13] G. A. Blake, "Microwave and terahertz spectroscopy," *Encyclopedia of Chemical Physics and Physical Chemistry*, eds. J. H. Moore and N. D. Spencer, Institute of Physics Publishing, London, 2001.

[14] P. J. Burke, R. J. Schoelkopf, D. E. Prober, A. Skalare, W. R. McGrath, B. Bumble and H. G. LeDuc, "Length scaling of bandwidth and noise in hot-electron superconducting mixers," *Appl. Phys. Lett.* **68,** 3344-3346 (1996).

[15] E. M. Gershenzon, M. E. Gershenzon, G. N. Gol'tsman, A. M. Lyul'kin, A. D. Semenov and A. V. Sergeev, "Electron-phonon interaction in ultrathin Nb films," *Sov. Phys. JETP* **70,** 505-511 (1990).

[16] P. L. Richards, "Bolometers for infrared and millimeter waves," *J. Appl. Phys.* **76,** 1-24 (1994).

[17] Lenses machined by Kadco Ceramics (Easton, PA) using high-resistivity float-zone silicon from Topsil Semiconductor Materials (Frederikssund, Denmark).

[18] D. J. Bendford, M. C. Gaidis and J. W. Kooi, "Optical properties of Zitex in the infrared to submillimeter," *Appl. Opt.* **42**, 5118-51122 (2003).

[19] Surfaceigniter Corp. (Chagrin Falls, OH), model 1034K

[20] M. Bin, D. J. Benford, M. C. Gaidis, T. H. Buttgenbach, J. Zmuidzinas, E. Serabyn and T. G. Phillips, "A large throughput high resolution Fourier transform spectrometer for submillimeter applications," *Int. J. IR and MM Waves* **20(3)**, 383-400 (1999).

[21] Future Instruments Corp. (College Park, MD), http://futureinstruments.com/

[22] G. Evans, D. C. Schmadel, A. B. Sushkov and H. D. Drew, "Silicon beamsplitter for Fourier transform spectroscopy at far infrared frequencies," *arXiv:0706.4302* (2007).

[23] A. Skalare, Th. de Graauw and H. van de Stadt, "A planar dipole array antenna with an elliptical lens," *Microwave and Opt. Tech. Lett.* **4**, 9-12 (1991).

[24] D. B. Rutledge, D. P. Neikirk and D. P. Kasilingam, "Integrated circuit antennas," *Infrared and Millimeter Waves* vol. 10, ed. K. J. Button, Academic Press, New York, 1983.

[25] J. D. Dyson, "The equiangular spiral antenna," *IRE Trans. Antennas Propagat.* **13**, 181-187 (1959).

[26] M. O. Reese, D. F. Santavicca, L. Frunzio and D. E. Prober, "Niobium hot electron bolometer development for a submillimeter heterodyne array camera," *IEEE Trans. Appl. Supercond.* **17(2)**, 403-406 (2007).

Erratum
Proc. SPIE 6772, 67720Q (2007).

In the first paragraph of section 5, the sentence

A dipole in a dielectric half space radiates power preferentially into the high dielectric material in proportion to the square root of the dielectric constant, so our antenna should couple with approximately 80% efficiency from the lens side of the device.[24]

should be corrected to read

A dipole in a dielectric half space radiates power preferentially into the dielectric material approximately in proportion to the dielectric constant to the power 3/2.[24]